Dansgaard-Oeschger Oscillations: A Hydrodynamic Theory

W. Richard Peltier[1] and Kotaro Sakai[2]

[1] Department of Physics, University of Toronto, Toronto, Ontario, Canada M5S 1A7
[2] Frontier Research System for Global Change, Seavans N., 7F, 1-2-1 Shibaura, Minato-ku, Tokyo, Japan 105-6791

Abstract: On the basis of the oxygen isotopic proxy for atmospheric temperature which has been measured in the GRIP and GISP2 deep ice-cores from Summit, Greenland, it is well known that climate in the North Atlantic sector of the planet was highly variable throughout the period of time conventionally referred to as Oxygen Isotope Stage (OIS) 3. This variability consists of millennium time-scale oscillations clustered in packets in which each successive oscillation has a somewhat smaller amplitude than the last. The time scale of individual packets is approximately 10 kyr. A hydrodynamic theory of the basic Dansgaard-Oeschger oscillation has been developed which comprises the millennium time-scale variability based upon a reduced model of the thermohaline circulation (THC). In the present paper the most recent results delivered by this hydrodynamic model are compared with those provided by a much simpler dynamical systems model based upon the assumption that the low-frequency time dependence of the THC may be described by interactions between the time evolving uniform salinities ascribed to each of three interacting boxes. The simple model is shown to agree remarkably well with the predictions of its more complicated hydrodynamic counterpart insofar as its qualitative behavior is concerned.

Introduction

The idea that sustained nonlinear oscillations of the thermohaline circulation might be responsible for the millennium time scale Dansgaard-Oeschger mode of climate variability which has been such an evident component of the thermal history of the North Atlantic sector of the climate system during the glacial period is one which has recently received a great deal of attention. Among the first of the papers in which this idea is contemplated was that by Broecker et al. (1990) in which an heuristic description of the concept of a "salt oscillator in the glacial Atlantic" was provided. Although their description as to how a process such as this might work was entirely qualitative, it nevertheless served to motivate a good deal of simultaneous and subsequent discussion. Broecker and Denton (1990), for example, focused upon the Younger Dryas climate reversal which interrupted the transition from full glacial to interglacial conditions. They ascribed this millennium time-scale cold phase, during which the climate system appears to have returned to the glacial state, to a "shutdown" of the process of North Atlantic Deep Water (NADW) formation caused by the massive outflow of freshwater onto the surface of the North Atlantic Ocean now known to have occurred during the preceding Bølling/Allerød warm period. Evidence for the required timing of this event is clear on the basis of the record from the North American continent (Teller 1987) which shows that it is at this time that the drainage of Glacial Lake Aggassiz was diverted from the Mississippi outlet to the St. Lawrence River outlet. It is also during the Bølling/Allerød warm period that sea level itself is known to have risen dramatically, primarily on the basis of the Barbados coral-based sea-level record by Fairbanks (1989) on the U/Th-based timescale by Bard et al. (1990).

These various pieces of the puzzle of millennium time-scale oscillation, although extremely interesting in themselves, have not led to any deep understanding as to how or why the sustained millennium time-scale oscillation evident in the Greenland ice-core records during Oxygen Isotope Stage 3 occurs. They do not clarify, for example, the question as to whether each os-

From *The Northern North Atlantic: A Changing Environment*, edited by P. Schäfer, W. Ritzrau, M. Schlüter, and J. Thiede, pp. 423–439, Springer, Berlin, 2001

cillation requires a separate pulse of freshwater to induce it. In fact, direct evidence exists to the effect that this is not the case and this is connected to the so-called Heinrich events (Heinrich 1988) which appear in North Atlantic deep-sea sedimentary cores as horizons with extremely high concentrations of ice-rafted debris. These events have been discussed in great detail by Bond et al. (1993) in relation to the GRIP and GISP2 oxygen isotopic records from Greenland. Correlations between them have been shown to reveal extraordinary structural relationships. In particular, individual Heinrich events appear to recur on a time scale of approximately 10 kyr and to occur simultaneously with an especially large amplitude Dansgaard-Oeschger (D-O) oscillation. Subsequent to this initial pulse, several further D-O oscillations are observed to occur, each with successively smaller amplitude, a process which continues until the next Heinrich event interrupts the sequence. Each of these Heinrich event initiated sequences of D-O oscillations is now commonly referred to as a Bond cycle.

The conventional understanding of the implications of these combined ice-core and marine observations has come to be based upon a scenario involving postulated interactions between the continental ice sheets which were in place over North America (the Laurentide ice sheet) and northwestern Europe (the Fennoscandian and Barents Sea ice sheets), and the deep-water formation process which is presently operating in the Greenland-Iceland-Norwegian Seas and the Labrador Sea. It is imagined that Heinrich events occur when the eastern flank of the Laurentide ice sheet experiences strong instability, resulting in the massive discharge of icebergs into the Atlantic through the Hudson Strait region. These icebergs are thought to be advected eastward, where they are eventually caught up in the North Atlantic Drift, thereafter moving northward, melting as they do so and covering the floor of the North Atlantic with ice-rafted debris (IRD) in consequence. The cap of freshwater which simultaneously forms over the surface ocean then causes the arrest of the NADW formation process and therefore the arrest of the deep thermohaline circulation itself. Since the process of deep-water formation leads to significant heating of the overlying atmosphere (100 W m^{-2} in the modern system on annual average), NADW shutdown leads to intense atmospheric cooling.

There are clearly a number of issues which must be considered in the process of assessing the reasonableness of this conventional wisdom. Perhaps foremost among these concerns is the question as to what causes ice-mechanical instability on the eastern flank of the Laurentide ice sheet which results in the observed Heinrich events. Furthermore, there is the question as to why, following each Heinrich event, a series of D-O oscillations develops, apparently in the absence of further instability of the ice mass. These issues appear to argue strongly for the primacy of the Dansgaard-Oeschger oscillation over the Heinrich events themselves, a conclusion to which Bond et al. (1997) have also been drawn. If the D-O oscillation does in fact constitute the primary mode of climate variability during OIS 3, Heinrich events may clearly be understood to constitute secondary features which are "phase entrained" to it. These massive ice-discharge events might then be understood to occur synchronously with every fourth or fifth D-O oscillation, the repeat time being determined by the time required for accumulation to return the eastern flank of the ice sheet to a state such that instability may be induced by the next oscillation.

If this alternative view of the climate variability of the North Atlantic sector of the climate system during OIS 3 is to be convincing, it clearly requires a mechanism for D-O oscillation which does not rely on *strong* coupling between it and ice-sheet mass. How otherwise are we to understand why D-O oscillations continue long after the preceding Heinrich event has ended? Previous work in this series has been directed precisely to the goal of understanding how the deep thermohaline circulation of the oceans might be influenced to "fibrillate" in the absence of explicit fibrillation of surface boundary conditions on temperature and salinity flux themselves. Beginning with the analyses presented in Sakai and Peltier (1993) a series of models of increasing complexity have been developed with which this question can be addressed. The first of this sequence of analyses which suggested the existence of a fluid mechanically viable theory was that presented by Sakai and Peltier (1995). A two-dimensional model of combined thermal and haline convection describing only the circulation of the Atlantic basin demonstrates that, when boundary conditions on temperature and precipitation minus evaporation are changed from those corresponding to modern climate to those which are believed to be characteristic of ice-age conditions, then the nature of the circulation was radically transformed. Under modern conditions, with diffusion coefficients for heat, salt and momentum chosen so as to permit the fitting of the approximately 18-Sv strength of modern Atlantic overturning flow, circulation was predicted to be only weakly variable with a dominant time scale of centuries and an amplitude of the variability of only 1–3 Sv. Under ice-age

boundary conditions, however, circulation was shown to become intensely oscillatory with a time scale of millennia and an amplitude equal to the modern-strength of the quasi steady flow itself. The lower case Circulation evolved quasi periodically, executing continuous spontaneous excursions between a state of strong overturning and a state of no overturning. Detailed analysis demonstrates that the change in boundary conditions which was primarily responsible for the onset of spontaneous oscillations was that of precipitation minus evaporation. In this analysis the representation of ice-age boundary conditions were elected so as to force the surface salinity of the Atlantic basin to be lower than modern salinities based upon foraminifera-based reconstruction by Duplessy et al. (1990). These analyses demonstrate that when a sufficiently high P-E anomaly is applied to the northernmost surface of the basin, where deep water would otherwise form in a quasi steady fashion, then circulation becomes intensely oscillatory on the millennium time scale. The predicted oscillation in heat transfer, however, does not take the form of smooth oscillations but rather of relatively long periods of weak transport followed by brief periods of intense thermohaline overturning.

This model was further developed in Sakai and Peltier (1996) to include several interacting basins, each of which was represented with a separate two-dimensional model of thermo-haline convection, linked hydraulically to its neighbors. The same bifurcation from steady to (Dansgaard-Oeschger) oscillatory convection was recovered in this multi-basin model as had been shown to occur in the single basin Atlantic model. However, the temporal structure of the oscillatory state was found to have the same "flush-collapse" form as had been found to occur in the single basin case. This "flush-collapse" nomenclature has been employed by both Weaver et al. (1993) and Winton and Sarachik (1993) to describe the very low-frequency variability observed in full three-dimensional models of thermohaline circulation in response to anomalous P-E although these authors did not seem to be aware of the Dansgaard-Oeschger oscillation. Weaver et al. (1993) believed the oscillation to be a numerical artifact, whereas Winton and Sarachik (1993) imagined that it might conceivably be connected to the Younger Dryas event.

A further publication on the theory of Dansgaard-Oeschger oscillation (Sakai and Peltier 1997) couples the multi-two-dimensional basin version of the model to an energy balance model of the atmosphere in order to estimate the extent to which the character of the "flush-collapse" oscillation may be modified by atmosphere-ocean feedback. These analyses, which will be briefly reviewed here, demonstrate that the influence of this feedback is profound. Under its influence, the "flush-collapse" oscillation was strongly modified into the same quasi periodic form as that exhibited by D-O oscillations in the oxygen isotopic records from the GRIP and GISP2 ice cores. Furthermore, because this model included an atmospheric component, it proved possible to make a specific prediction of the oscillation of atmospheric temperature over the region in which deep water forms which should accompany the oscillation in circulation strength. These analyses predicted a peak-to-peak variation of amplitude of approximately 6 °C, a number which rather precisely fits the observed temperature signal based upon application of the calibration by Johnsen et al. (1992) to isotope records from the Greenland cores. This result has been construed to provide rather definitive proof that thermohaline circulation would indeed be expected to "fibrillate" under boundary conditions thought to have been characteristic of glacial conditions. Because the previously referenced three-dimensional thermohaline circulation analyses deliver the same "flush-collapse" oscillation as the two-dimensional model, nothing fundamental appears to have been omitted by using the initial versions of this theory based on two-dimensional thermohaline circulation models.

In the most recently published analyses with this model (Sakai and Peltier 1998) further focus has been placed upon the detailed behavior of THC during the most recent glacial-interglacial transition. Probably the most enigmatic aspect of the ice-core inferred details of this period concerns the Bølling/Allerød warm precursor to the Younger Dryas cooling event. Clearly, if the Younger Dryas event is indeed to be thought of as the forced response of the thermohaline circulation to intense freshwater loading of the surface of the North Atlantic during the preceding Bølling/Allerød period, then THC must have been fully "off" prior to the Bølling and have been reinvigorated during the Bølling itself. This suggests that it should also have been "off" or at least significantly reduced at glacial maximum. This is entirely consistent with our explanation of D-O oscillation which existed during OIS 3, an epoch which ended prior to LGM, in that THC during that period was in a state of fibrillation in which it oscillated between full on and full off conditions in response to a high-latitude Atlantic excess buoyancy flux associated with a quasi steady run-off derived anomaly supported by land-based reservoirs of freshwater provided by the Laurentide and northwest European ice sheets. In order for this scenario to be reasonable, the THC at LGM at

21 kyr BP must have been relatively quiescent, in accord with ice-core data which reveal no D-O oscillations late in OIS 2. In Sakai and Peltier (1998) the complete to have ocoured sequence of observed climatic events from LGM to the present may be reproduced if the total freshwater anomaly is divided into two components, one which is directly related to the variation of sea level and one which is not related to sea level but rather to a shift in the hydrological cycle which occurs once a sufficiently large Laurentide ice sheet is emplaced on the North American continent. Insofar as the latter component of the anomaly is concerned, ice sheets simply serve as a "collector" of fresh water, part of which is then directly delivered to the North Atlantic as run-off rather than contributing to ice-sheet growth. The fact that the ice sheets are sensibly imagined to play this role of intermediary is consistent with observations of global sea-level rise during OIS 3 provided by the coral-based record from the Huon Peninsula, Papua New Guinea by Chappell et al. (1996) and deep-sea sedimentary core-derived records by Shackleton (1987). During OIS 3, the period in which intense D-O oscillations are observed in the GRIP and GISP2 ice cores, mean sea level is not observed to have continued to fall significantly. Rather, the precipitation which continued to fall on the North American ice sheet appears to have been lost to the oceans. This run-off contribution to effective P-E explains the existence of the D-O oscillation during OIS 3.

Our explanation for the detailed sequence of events which occur during this period, however, requires that this run-off component also consist of two distinct contributions, one which is quasi steady and is not linked to sea level and another which has a direct connection to sea-level variability. The *existence* of the D-O oscillation does not require any time variability in the high-latitude freshwater anomaly. However, the modulation of this oscillation which is required to produce the Bond cycle is most easily understood by imagining that individual Heinrich events add a time dependence to the background freshwater anomaly which does directly influence sea level, although most probably not (according to the Huon Peninsula data) to any significant degree.

In the following section of this paper, the structure of the multi-two-dimensional basin model of the THC which has been developed to illustrate the manner in which the D-O oscillation of THC strength may be produced by adding an appropriate perturbation to P-E over the region in which deep water would otherwise form will be briefly reviewed. In the section entitled "A Three-Box Model with a Hopf Bifurcation" it is shown that the physics which underlies the onset of oscillatory behavior may also be captured in a simple three-box model of circulation which is similar to that originally introduced by Stommel (1961). This simpler model provides a vehicle in terms of which it is possible to explicitly describe a scenario for the OIS 3 Bond cycle. The conclusions which follow from the sequence of analyses described herein are summarized in the Conclusions.

A Multi-Two-Dimensional Basin Model of Thermohaline "Fibrillation"

The dimensionally reduced hydrodynamic model developed to illustrate the mechanics of Dansgaard-Oeschger oscillation consists of two fundamental components, a model of the deep circulation of the oceans and a model of the response of the overlying atmosphere to changes in this circulation and of the feedback of this response onto the model ocean. These two coupled ingredients are themselves subcomponents of a more extensive modeling structure which is being developed to understand the full spectrum of climate variability throughout the latter half of the Pleistocene epoch, during which time the dominant mode of climate variability consisted of the 100-kyr quasi periodic variation of continental ice-sheet volume apparently forced by Milankovitch variations of orbital insolation. Recent work by the Toronto group on this lower frequency mode of climate variability is described in Deblonde and Peltier (1991, 1993), Peltier and Marshall (1995) and Tarasov and Peltier (1997, 1999). In the following subsections focus will be placed upon the two components required to understand the D-O oscillation and on the interactions which underlie the oscillation itself.

Thermohaline Circulation

The geometry of the ocean general circulation model which has been developed for the purpose of analyzing the low-frequency variability of THC is illustrated in Figure 1. Each of the four major ocean basins is assumed to be two-dimensional, three of which are north-south oriented (Atlantic, Pacific and Indian Oceans), while the fourth (the Southern Ocean) is zonal. The complete structure then takes the "flywheel" form shown. In each of these basins circulation is described by 3 prognostic variables, those of stream function, temperature and salinity. The simultaneous set of partial differential equations which link these three prognostic variables, for any one of the north-south oriented basins, is as follows:

$$\left(\nu_V \frac{\partial^2}{\partial r^2} + \frac{2\nu_V}{r}\frac{\partial}{\partial r} + \frac{\nu_V}{r^2}\frac{\partial^2}{\partial \theta^2} + \frac{\nu_H \cot\theta}{r^2}\frac{\partial}{\partial \theta} \right) \omega = \frac{-g}{\rho_o}\frac{\partial \rho}{\partial \theta} \quad (1)$$

$$\left(\frac{\partial^2}{\partial r^2} + \frac{1}{r^2}\frac{\partial^2}{\partial \theta^2} - \frac{\cot\theta}{r^2}\frac{\partial}{\partial \theta} \right) \Psi = -\rho_o \Gamma \omega \sin\theta \quad (2)$$

$$\frac{\partial T}{\partial t} = \frac{-1}{\rho_o r^2 \sin\theta} J(T, \Psi) + \left(K_{TV}\frac{\partial^2}{\partial r^2} + \frac{2K_{TV}}{r}\frac{\partial}{\partial r} + \frac{K_{TH}}{r^2}\frac{\partial^2}{\partial \theta^2} + \frac{K_{TH}\cot\theta}{r^2}\frac{\partial}{\partial \theta} \right) T \quad (3)$$

$$\frac{\partial S}{\partial t} = \frac{-1}{\rho_o r^2 \sin\theta} J(S, \Psi) + \left(K_{SV}\frac{\partial^2}{\partial r^2} + \frac{2K_{SV}}{r}\frac{\partial}{\partial r} + \frac{K_{SH}}{r^2}\frac{\partial^2}{\partial \theta^2} + \frac{K_{SH}}{r^2}\cot\theta\frac{\partial}{\partial \theta} \right) S \quad (4)$$

in which the Jacobian operator $J(f, \Psi) = (\partial\psi/\partial r)(\partial f/\partial\theta) - (\partial\Psi/\partial\theta)(\partial f/\partial r)$ and the density ρ is determined by the following approximation to the full nonlinear equation of state suggested by Winton and Sarachik (1993):

$$\rho(T, S) - 1 = 7.968 \cdot 10^{-1} s - 5.59 \cdot 10^{-5} T - 6.3 \cdot 10^{-6} T^2 + 3.7315 \cdot 10^{-8} T^3 \quad (5)$$

in which ρ is in kilograms per cubic meter, s is in grams per kilogram and T is in degrees Celsius. The two-dimensional model of the Southern Ocean through which the individual north-south oriented basins described by systems of equations of the form (1)–(4) are hydraulically linked is described by a similar set of equations (those numbered [11]–[18] in Sakai and Peltier 1997). No useful purpose is served by rewriting this system here. In the system (1)–(5) the coefficients $\nu_{V,H}$, $K_{TV,H}$, $K_{SV,H}$ are the vertical (V) and horizontal (H) diffusion coefficients for momentum, heat and salt, explicit values for which are listed in Table 2 in Sakai and Peltier (1996). It is a consequence of the fact that the horizontal diffusivities are orders of magnitude greater than the vertical diffusivities that overturning circulation in the "thin" oceanic layer, thin compared to the pole-to-pole horizontal extent, is regularized in the sense that the radial (r) and latitudinal (θ) derivative terms in equations (1), (3) and (4) are made comparable in magnitude and the individual elliptic operators simple to invert using standard multi-grid software. It is important to note that the vorticity and stream function equations (1) and (2) are approximate forms which, under the assumption that the inertial force may be neglected in the balance of momentum, obtain in an approximation which is rigorously justifiable only in the limit of high effective Prandtl numbers or very slow time dependence. In the present context the validity of this approximation is most easily justifiable a posteriori in consequence of the very low frequency of the phenomenology discussed here.

In Sakai and Peltier (1995, 1996) the manner in which this model was tuned so as to enable it to fit the properties of the modern thermohaline circulation in the Atlantic basin are described. For the surface boundary conditions over each of the individual basins sea-surface air temperature data sets by Schutz and Gates (1971) and precipitation minus evaporation data by Baumgartner and Reichel (1975) have been employed. Values for the vertical and horizontal diffusivities for heat and salt and the vertical diffusivity for momentum were then fixed to those employed in a standard low-resolution three-dimensional ocean general circulation model such as the Princeton MOM. Because the 2-D models cannot directly describe the important impact of the Coriolis force upon circulation, which in the ocean interior is almost perfectly balanced by the horizontal pressure gradient (so-called geostrophic balance), the horizontal diffusivity for momentum must be significantly increased above the level which would be required in a 3-D model in which the Coriolis force plays an important role. This does not seem to be an overly severe restriction on the validity of a two-dimensional model of Atlantic overturning circulation, however, since north-south transport is primarily effected in the narrow western boundary current, the existence of which depends upon Coriolis control. It is, in effect, a consequence of the global impact of the Coriolis force that THC assumes the "loop circulation" form which may be adequately described by ignoring the Coriolis force entirely! In tuning the 2-D model of the THC to modern circulation patterns, the only remaining parameter, horizontal momentum diffusivity, has simply been chosen such that a mean strength for the overturning circulation of approximately 18 Sv is obtained.

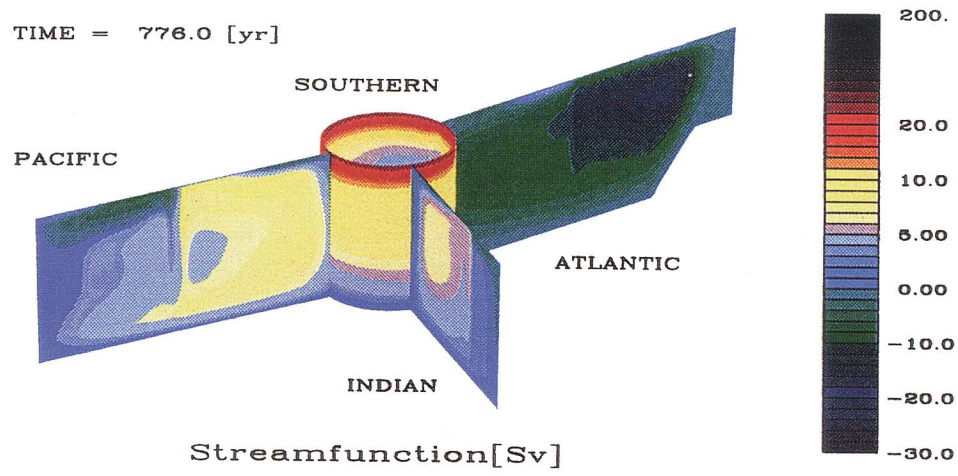

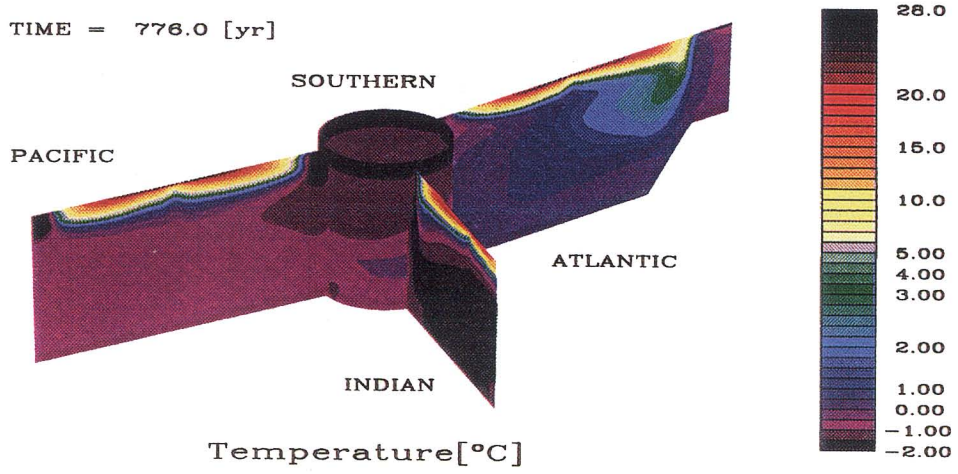

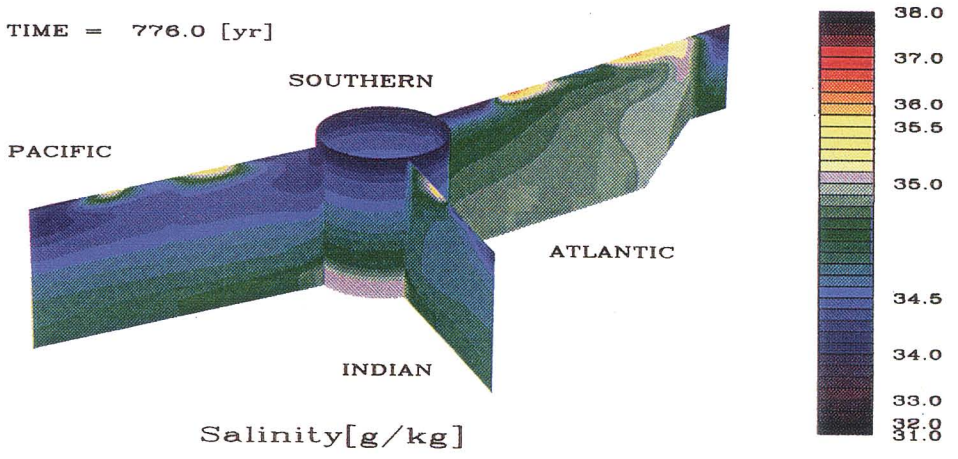

Fig. 1: The geometry of the multi-two-dimensional-basin reduced model of global thermohaline circulation showing stream function (top), temperature (middle) and salinity (bottom) in each of the four basins which comprise the model. The results are shown for one instant of time in what is in fact a (perhaps strongly) time-dependent flow

As discussed at much greater length in Sakai and Peltier (1996), the ocean-only form of the model then delivers a circulation pattern whose other properties are also reasonable facsimiles of modern observations and of the Holocene record of THC strength assumed to be provided by $\delta^{18}0$ observations from the Greenland ice cores. In the former connection the model predicts the existence of thermal and salinity boundary layers at the upper surface of the ocean on the order of 1 km thick. In the latter connection the model also predicts that the strength of the circulation in the Atlantic basin is only weakly variable in time, exhibiting peak-to-peak oscillations in stream function extrema of only about 1–2 Sv (see Fig. 3 in Sakai and Peltier 1997). As will be clear by inspection of Figure 1, the model also includes a parameterization of the influence of the wind-driven circulation through an Ekman pumping representation. It should also be understood that the convective instability through which deep water actually forms is not fully resolved by this model, but must also be parameterized through the use of a standard convective adjustment scheme. This is a consequence of the fact that the horizontal scale of individual boundary layer instability events, during which surface water is subducted to depth, is extremely small. Observations suggest that these scales are only on an order of a few kilometers at most (e.g. Killworth 1976). Given that the pole-to-pole extent of the Atlantic basin of the model is in excess of 10,000 km, it is clear that the global use of a horizontal grid spacing adequate to resolve these individual boundary layer instability events involved in NADW formation would be prohibitive.

The Atmospheric Response

In the atmosphere-ocean coupled structure developed here, the atmosphere is represented using a simple energy balance model. This model is, in fact, global in scope and evolves the surface energy balance according to the following partial differential equation for surface temperature $T(\underline{r}, t)$:

$$C(\underline{r}, t)\frac{\partial T(\underline{r}, t)}{\partial t} = \underline{\nabla}_h \cdot \left[D(\theta)\underline{\nabla}_H T(\underline{r}, t) \right] + A + B\left[T(\underline{r}, t) - T_{topo}(\underline{r}, t) \right] + \frac{Q}{4} a(\underline{r}, t) S(\theta, t) + NAHF \quad (6)$$

In (6) $C(\underline{r}, t)$ is surface heat capacity which is employed to distinguish surface type on the surface of the spherical earth (land having low C and oceans high C), and $D(\theta)$ is a diffusion coefficient whose influence is intended to represent the (highly non-diffusive) heat transport effected by baroclinic eddies in the atmosphere. The second term on the right-hand side of (6) is a linear approximation to the temperature-dependent infrared emission to space, whereas the last term represents incident solar insolation with solar constant $Q = 1360$ W m^{-2} and solar distribution function S mediated by the surface albedo $a(\underline{r}, t)$. The last term in (6), *NAHF*, represents the heat transferred to the atmosphere by the deep-water formation process in the North Atlantic Ocean. This heat transfer will clearly modify surface temperature, which is an important boundary condition for the overturning circulation of the oceans, and it is therefore through this term that oceanic and atmospheric components are coupled.

The scheme which is actually employed to couple those two components of the structure is asynchronous and has been described in detail in Sakai and Peltier (1997). Every 20 years a new equilibrium annual cycle of atmospheric temperature is computed and, after appropriate spatial averaging, this surface temperature field is employed to provide boundary conditions on this field on the surface ocean for the next 20 years of integration of the ocean model. This new annual cycle is computed subject to the *NAHF* delivered by the ocean model prior to the time of update. In time-stepping the ocean model explicitly through a period of 20 years the old temperature boundary condition is relaxed towards the new annual cycle so as to ensure the stability of the asynchronous coupling procedure. Further details of this procedure are described in schematic form in Figure 2 in Sakai and Peltier (1997).

One property of this model which is of particular interest in the present connection is that the hydrological cycle is not described explicitly. Rather, P-E over the oceans is prescribed as being equal to that which obtains at present, in addition to a departure selected to represent the state of the climate system at some epoch in the past. The basis upon which this departure is selected is, of course, critical to assessing the reasonableness of the climate change scenario which the model then predicts. A discussion of results intended to mimic the climate variability observed to be characteristic of OIS 3 in the GRIP and GISP2 deep-ice cores from Greenland now follows.

Dansgaard-Oeschger Oscillation in the Coupled Model

Figure 2 shows a bifurcation diagram for the coupled model in which the characteristic period of the time de-

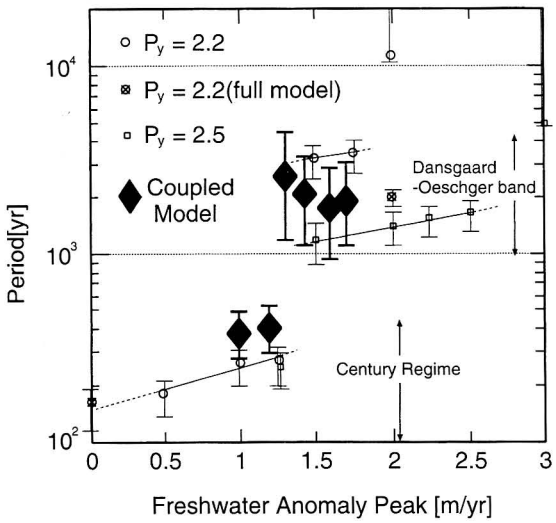

Fig. 2: Bifurcation diagram illustrating the dependence of the characteristic time scale of the temporal variability of circulation as a function of the maximum intensity of the Gaussian-shaped anomaly in P-E applied over the northern part of the North Atlantic basin of the model where the most intense rate of formation of deep water would otherwise occur. The results denoted by the small symbols were obtained for the oceans-only version of the model described in Sakai and Peltier (1996), whereas those for the atmosphere-ocean coupled model described herein are denoted by solid diamond symbols

pendence of circulation, determined on the basis of power spectra of the stream function maximum, is plotted as a function of the magnitude of the departure of P-E from that in the modern climate system thought to have existed during OIS 3 over the North Atlantic. This anomaly is assumed to be of Gaussian shape as a function of latitude and is centered over the North Atlantic at 50° N latitude and characterized by a width of 10° latitude. Since the anomaly consists of an excess of precipitation over evaporation and since no net imbalance into the water cycle is to be introduced for the purpose of these experiments, P-E has been decreased over the remaining basins by a constant amount so as to preserve balance for the purpose of OIS 3 simulations. The results from the coupled model are shown on Figure 2, as bold diamond-shaped symbols, compared to the equivalent results for the ocean-only version of the model described in Sakai and Peltier (1996), which are distinguished by different values of a parameter P_y that was employed earlier to represent the depression of temperature near the poles obtained under ice-age conditions. It is very clear on the basis of inspection of this Figure that, when the peak value of the Gaussian freshwater anomaly exceeds approximately 1.25 m yr^{-1}, the variability of THC is radically transformed. Whereas for low values of the maximum perturbation, variability occurs on the century time scale, above the critical value the time scale increases into the millennium-scale Dansgaard-Oeschger band. Apart from this marked change in time scale of the internal variability, other properties of THC are also transformed.

One additional aspect of this transformation will be clear on the basis of Figure 3, which shows the manner in which meridional heat transport in the North Atlantic basin of the model across 30° N latitude changes as the peak freshwater anomaly increases through the sequence 1 m yr^{-1}, 1.2 m yr^{-1}, 1.35 m yr^{-1}, 1.45 m yr^{-1}, 1.8 m yr^{-1}, 1.7 m yr^{-1} and 2 m yr^{-1}. In this diagram negative values for heat transport imply that the transfer is northwards. Inspection of this Figure shows that for weak anomalous freshwater forcing heat transport remains weakly variable on the century time scale about a large negative value, implying that THC is in the "full-on" mode in which NADW steadily forms in the north Atlantic and flows southwards along the floor of the basin. As the magnitude of maximum perturbation crosses the 1.25 m yr^{-1} threshold, however, heat transport begins to episodically collapse from the full-on value of about $4 \cdot 10^{14}$ W to zero. Over the 30 kyr sample of the synthetic heat transport time series shown, approximately 17 such collapses occur, and, following each, flow returns to its "full-on" state. With further increases in the strength of the anomaly, oscillations at first become somewhat more regular, but the solution comes to assume the form of millennium time-scale excursions from the off-state to the on, rather than the converse structure which characterizes the weakly perturbed regime. For the most strongly perturbed sample-time history with peak forcing of 2 m yr^{-1}, heat transport falls to zero and remains there as THC has entirely collapsed.

The sequence of events which occurs in this coupled model of the Atlantic THC is strongly indicative of the occurrence of a Hopf bifurcation in the dynamical system for supercritical values of anomalous freshwater forcing. A range of amplitudes of the anomaly clearly exists, within which circulation is intrinsically oscillatory, a range which is not particularly broad and which is only slightly weaker than what is required to cause the complete arrest of circulation. It might be interesting for the reader unfamiliar with nonlinear dynamical systems of this kind to know that such behavior is in fact rather common. In the related problem of pure thermal convection, for example, an intensely oscillatory mode exists for thermal Rayleigh numbers sufficiently high to induce time-dependent behavior (e.g. Solheim and Peltier 1990). It was in fact the knowledge of such be-

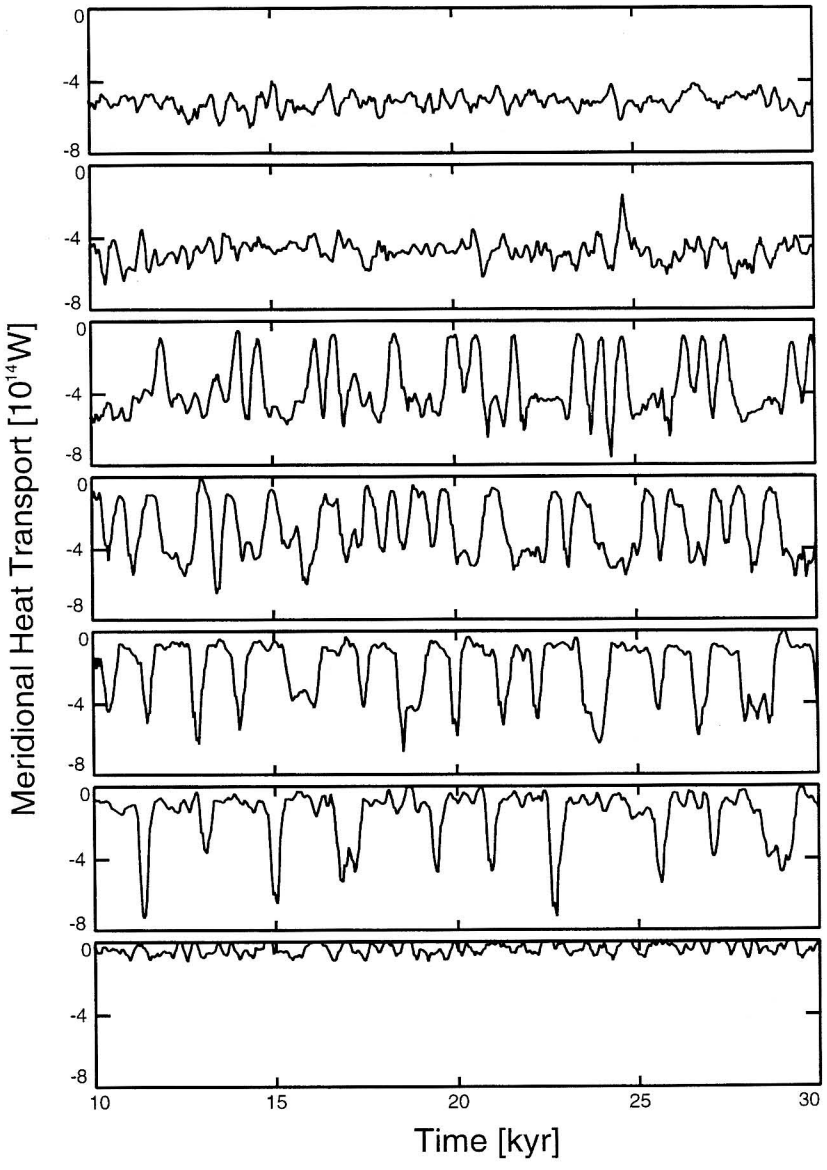

Fig. 3: Meridional heat transport in the Atlantic basin of the coupled atmosphere-ocean model across 30° N latitude. A negative value for heat transport implies that transport is northwards. The raw data output in the model have been smoothed by application of a 200-year moving average to the raw data. The seven frames in the Figure display results (top to bottom) for peak values of the Gaussian P-E perturbation applied to the North Atlantic basin of 1, 1.2, 1.35, 1.45, 1.6, 1.7 and 2 m yr^{-1}

havior in this analogous problem that led to the theory of D-O oscillation that we have been developing.

A further characterization of this bifurcation in behavior is presented in Figure 4, in which, for the same sequence of peak amplitudes in the anomalous component of freshwater flux, sea-surface air temperature over the Atlantic at 50° N is determined by applying a 200-year moving average to the raw data delivered by the atmospheric component of the coupled model. Results are shown for both the summer and winter seasons for each of the different experiments. It is clear from inspection of these results that surface air temperature is high when THC is in the "on" state, and low when it is "off". As is also clear by inspection of the heat transport data in Figure 3, for increasing values of the strength of freshwater perturbation within the Dansgaard-Oeschger oscillatory regime, the period of oscillation increases somewhat, reaching approximately 3 kyr before variability ceases with the complete collapse of circulation. Of greatest interest in Figure 4, however, is the peak-to-

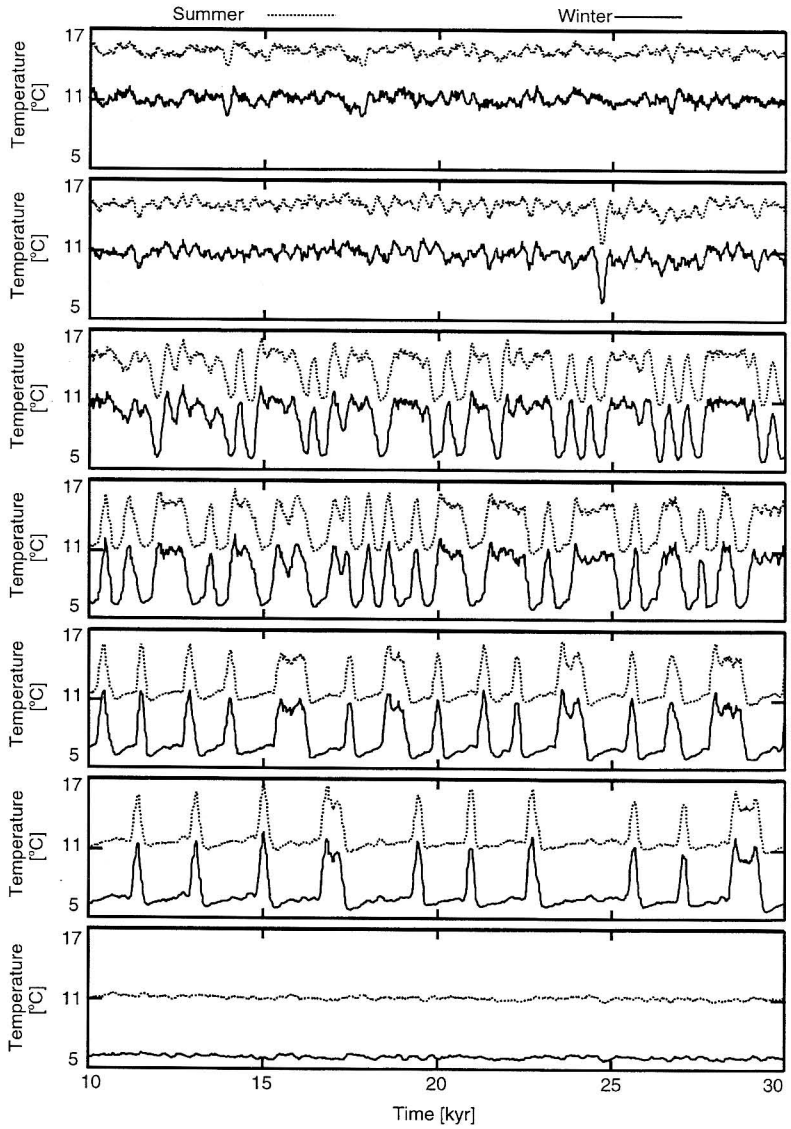

Fig. 4: Sea-surface temperature over the North Atlantic at 50° N latitude corresponding to integrations of the model for the same set of peak values of the P-E anomaly employed for meridional heat transport data shown in Figure 3. For each integration, results are shown for both the summer and winter seasons, and these results have been obtained by applying the same 200-year moving average to raw data as employed to construct Figure 3

peak variation in atmospheric temperature which characterizes each individual oscillation. The value of 6 °C evident from the Figure appears to be fully consistent with the conventional calibration of the $\delta^{18}0$ signal in the Greenland ice-cores by Johnsen et al. (1992).

Given the relative simplicity of the above-described mechanism for Dansgaard-Oeschger oscillation it does not seem unreasonable to expect that the physical process may be described in terms of an even simpler mathematical structure which does not require the solution of such a complex set of coupled nonlinear partial differential equations. If such a further reduced model could be shown to exist it might also prove useful in understanding the complete sequence of events which occurs in the Bond cycle. In the following section of this paper such a model will be discussed.

A Three-Box Model with a Hopf Bifurcation

The application of simple box model representations of THC has had a distinguished history, beginning

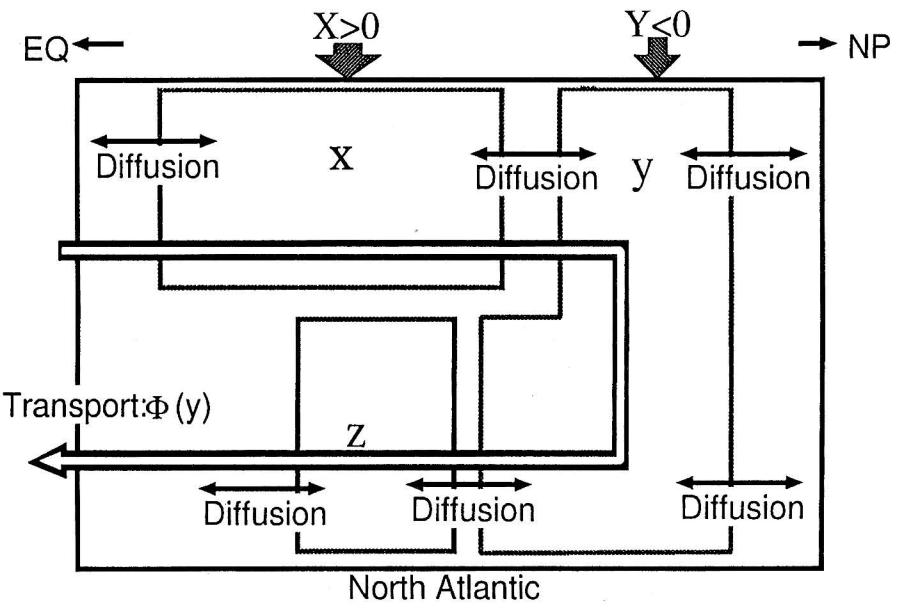

Fig. 5: Schematic overview of the three major sub-domains into which the North Atlantic Ocean has been divided for the purpose of constructing the "box-model" of thermohaline circulation

with a paper by Stommel (1961) showing that thermohaline circulation is capable of existing in two different steady circulation regimes under the same surface boundary conditions. This was one of the first examples of the concept of multiple-equilibria applied to a problem in geophysical fluid dynamics. In this Section it will be shown that all of the basic phenomenology revealed in the previous model based upon the complete set of hydrodynamic equations which describe the process of thermohaline convection may be recovered in a simple box model structure of this kind in which the dynamics are described by a small number of simultaneous nonlinear ordinary differential equations.

The basic three-box model that will be employed to demonstrate this fact is illustrated in Figure 5 in which the North Atlantic basin is shown as being divided into three basic water masses. These are, respectively, a near-surface mid-low-latitude water mass, a water mass which extends from the surface to the abyss in the northern part of the basin where deep water forms, and a water mass which represents abyssal water in the remainder of the basin. These water masses are assumed to exchange properties both diffusively and by the direct influence of advection. It is furthermore assumed that it is the salinity of the individual water masses which is the primary determinant of their density insofar as exchange processes are concerned. Denoting by s_1, s_2 and s_3 the salinities of these three (individually well mixed) boxes, it is possible to immediately write the evolution equations for salinity, in the spirit of Stommel (1961), as:

$$\frac{ds_1}{dt} = R_1 - K(s_1 - s_{bg}) - L(s_1 - s_2) - \Phi(s_2)(s_1 - s_{bg}) \tag{7}$$

$$\frac{ds_2}{dt} = R_2 - 2K(s_2 - s_{bg}) - L(s_2 - s_1) - L(s_2 - s_3) - \Phi(s_2)(s_3 - s_1) \tag{8}$$

$$\frac{ds_3}{dt} = -K(s_3 - s_{bg}) - L(s_3 - s_2) - \Phi(s_2)(s_3 - s_2) \tag{9}$$

According to this system of equations, then, both s_1 and s_2 are externally forced at rates R_1 and R_2 by direct contact with the atmosphere. The surface equatorial box also exchanges salinity both with a background reference level s_{bg} and with the high-latitude box, the high-latitude deep-water box exchanges diffusively both with the background and with the other two boxes, while the abyssal water mass exchanges diffusively both with the background and with the high-latitude box. The advective exchange between the boxes described by the transport function Φ is assumed to have a strength which depends only upon the salinity of high-latitude box s_2 relative to the assumed constant background value. Its net influence upon the salinity of the three boxes is as-

sumed, furthermore, to be linearly proportional to appropriate salinity differences. As will be clear by inspection of (7)–(9), the inter-box diffusion coefficients are all assumed to have the same value, namely L, whereas the diffusion coefficient which determines exchange between individual boxes and the background is taken to be K. The factor of 2 which appears in the second term on the right-hand side of (8) is introduced for mathematical convenience and plays no fundamental role. The transport function Φ is assumed to depend upon the salinity in the high-latitude box as:

$$\Phi(s_2) = \begin{cases} \alpha |s_2 - s_{bg}|^{\beta} & \text{if } s_2 > s_{bg} \\ 0 & \text{otherwise} \end{cases} \tag{10}$$

implying that advective modification of the salinity field will occur only if the salinity of the high-latitude box s_2 exceeds that of the background. That a dependence of this sort should obtain is clear on the basis of the fact that no thermohaline circulation will exist unless deep water forms, and for this to occur the salinity of the high-latitude box must be sufficiently high. It is important to understand, in this context, that at high latitudes where surface temperatures are low the density of sea water is much more strongly controlled by salinity than it is by temperature. The parameter β, which may exceed unity, determines the strength of the dependence of the rate of circulation upon this salinity difference.

The solutions of the system (7)–(9) may be most economically catalogued if the equations are first nondimensionalized. This may be most simply accomplished by introducing new dependent variables x, y, z such that $s_1 - s_{bg} = s_o x$, $s_2 - s_{bg} = s_o y$ and $s_3 - s_{bg} = s_o z$ and choosing to nondimensionalize time in terms of a scale τ such that $t = \tau t^*$ (with t^* the nondimensional time) such that $\tau = (K + L)^{-1}$. Further defining the parameters $\mu = L/(K+L)$ and $s_o^{\beta} = (K+L)/\alpha$ the system (7)–(9) reduces to:

$$\frac{dx}{dt^*} = X - x + \mu y - |y|^{\beta} x \tag{11}$$

$$\frac{dy}{dt^*} = Y - 2y + \mu(x+z) + |y|^{\beta}(x-z) \tag{12}$$

$$\frac{dz}{dt^*} = -z + \mu y + |y|^{\beta}(y-z) \tag{13}$$

where clearly, on the basis of (10), the terms which include the factor $|y|^{\beta}$ are assumed to vanish when y is negative. Physical arguments lead to estimates for τ which may range from decades to millennia, whereas the parameter μ is expected to lie in the range between 0 and unity with an expected value near 0.5.

The nondimensional forcing terms in (11) and (12), namely X and Y, are clearly constrained with respect to sign on the basis of observations of the variation of the P-E distribution over the surface of the North Atlantic Ocean. X represents salinity forcing over low-middle and equatorial latitudes where very strong evaporation is induced by subtropical atmospheric divergence, so X should be large and positive. Y, on the other hand, represents salinity forcing over the high-latitude North Atlantic, where the combined influence of precipitation and surface run-off from the surrounding continents produces a negative salinity forcing and so Y must be negative. In attempting to constrain the magnitudes of these forcing functions it is important to realize that the overall salinity of the oceans remains close to the value of 0.035 g/kg and that the THC is, therefore, actually driven by rather small salinity differences, typically by relative differences on an order of 10^{-1} or even 10^{-2}. This directly implies that the magnitudes of X and Y should be close to the inverse of these relative differences, namely on an order of 10^1 or 10^2. As will be shown, the nature of the solutions to the system (11)–(13) is not determined by the separate magnitudes of X and Y but only by the ratio Y/X as might be expected on physical grounds.

Insights into the nature of these solutions may be obtained in the usual way for models of this kind by first focusing upon the equilibria which they allow. These equilibria are clearly such that $dx/dt^* = dy/dt^* = dz/dt^* \equiv 0$ so that x, y and z are themselves such that

$$0 = X - x - \mu y - |y|^{\beta} x \tag{14}$$

$$0 = Y - 2y + (x+z) + |y|^{\beta}(x-z) \tag{15}$$

$$0 = -z + \mu y + |y|^{\beta}(y-z) \tag{16}$$

In the case in which $y < 0$, $|y|^{\beta} \equiv 0$ by construction so that the system (14)–(16) is linear and has the simple solution

$$x_{ol} = \frac{2 + \mu Y - \mu^2 X}{2(1-\mu^2)} \tag{17}$$

$$y_{ol} = \frac{Y + \mu X}{2(1-\mu^2)} \tag{18}$$

$$z_{ol} = \frac{\mu(Y + \mu X)}{2(1-\mu^2)} \tag{19}$$

For this solution to remain physical with $y_{ol} < 0$ we must clearly have $Y + \mu X < 0$ since $0 < \mu < 1$. The physical implication of the condition $Y + \mu X < 0$ is that when

it obtains the high-latitude surface of the Atlantic receives too much freshwater to permit the maintenance of a strong THC. The stability of this linear equilibrium solution is determined by seeking solution vectors $(x, y, z)\ \alpha\ e^{\lambda t}$ to derive the characteristic equation for λ as:

$$(\lambda + 1)(\lambda^2 + 3\lambda + 2 - 2\mu^2) = 0 \qquad (20)$$

This equation has no roots $\lambda > 0$ so that the linear equilibrium solution is always stable.

For the more complex nonlinear equilibria with $y \geq 0$ the solutions to (14)–(16) are

$$x_{on} = \frac{X + \mu y}{1 + y^{\beta}} \qquad (21)$$

$$z_{on} = \frac{\mu y + y^{\beta+1}}{1 + y^{\beta}} \qquad (22)$$

with y_{on} a solution to the following nonlinear algebraic equation:

$$y_{on}^{2\beta+1} + (2 - \mu)\, y_{on}^{\beta+1} - (Y + X)\, y_{on}^{\beta} + 2(1 - \mu^2)\, y_{on} - (Y + \mu X) = 0 \qquad (23)$$

With $\beta = 1$ (23) is a simple cubic and may be solved analytically using Cardan's formula (e.g. Uspensky 1948). In general, however, (23) must be solved numerically, and under these circumstances we are interested only in physically admissible solutions characterized by $y_{on} > 0$.

Give an admissible nonlinear equilibrium solution (x_{on}, y_{on}, z_{on}) determined by solving (21)–(23), its stability may be determined once more by perturbing the equilibrium by small amplitude fluctuations (x', y', z'), substituting the perturbed solution into the governing equations (11)–(13) and linearizing in the perturbations. Once more seeking solutions $(x', y', z')\ \alpha\ e^{\lambda t}$ the following characteristic equation is obtained for λ:

$$(\lambda + 1 + y_{on})(\lambda^2 + \alpha_1 \lambda + \alpha_2) = 0 \qquad (24)$$

with

$$\begin{aligned} \alpha_1 &= 3 + y_{on} + z_{on} - x_{on} \\ \alpha_2 &= (1 + y_{on})(1 + z_{on} - x_{on}) \\ &\quad - (\mu - x_{on})(\mu - y_{on}) \\ &\quad - (\mu - y_{on})(\mu + 2\mu_{on}) \end{aligned} \qquad (25)$$

Clearly one of these eigenvalues is negative when $y_{on} > 0$ and such that $\lambda = -1 - y_{on}$. The remaining 2 eigenvalues are also negative if $\alpha_1 < 0$ and $\alpha_1^2 < 4\alpha_2$ if $-\alpha_1 + (\alpha_1^2 - 4\alpha_2)^{1/2} < 0$. In circumstances in which a λ exists with a positive real part this generally means, given no stable solution, that time-dependent solutions will be obtained under time integration of the dynamical system that may consist of periodic limit cycles or deterministically chaotic orbits. The following will show that this dynamical systems model delivers limit cycle solutions of D-O type for values of the Y/X ratio such that high-latitude freshening is only slightly less than that required to cause the THC to collapse. This will suffice to demonstrate that even this simple box model delivers the same facsimile of the D-O oscillation as discussed in the previous section on the basis of the detailed hydrodynamic model.

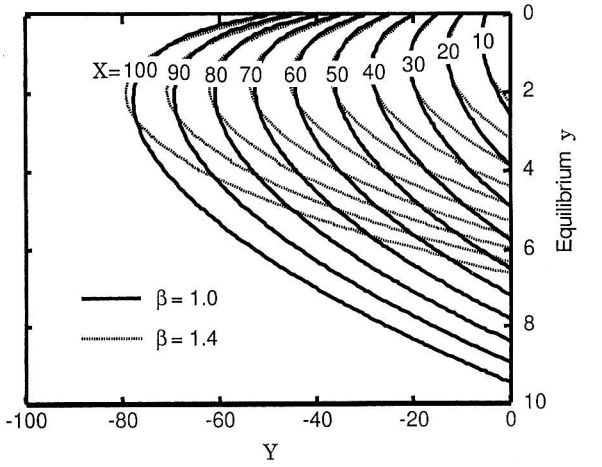

Fig. 6: Multiple equilibrium solutions for the deep-water production rate "y" as a function of P-E forcing applied to equatorial and high-latitude surface boxes X and Y. Results are shown for two different choices of the parameter β which determines the strength of the dependence of the transport function Φ on the difference between the salinity of the high-latitude surface box and the background value

In Figure 6 nonlinear equilibrium solutions, represented by y, are plotted as a function of X and Y in the range $0 \leq X \leq 100$, $-100 \leq Y \leq 0$ for two values of $\beta = 1.0$ and 1.4. Inspection will demonstrate that, for a wide range of X, Y combinations, two values of y exist which are possible equilibria. Such equilibrium solutions may be classified into three distinct categories. Those solutions with $y < 0$ are solutions with no NADW formation and therefore no THC, and define a stagnant regime. The other two categories both have $y > 0$ and comprise the two solutions which may simultaneously exist according to Figure 6, one of which corresponds to intense NADW formation (largest y) and one of which corresponds to weak NADW formation (smallest y). The latter solution is always unstable and does not, therefore, warrant further discussion.

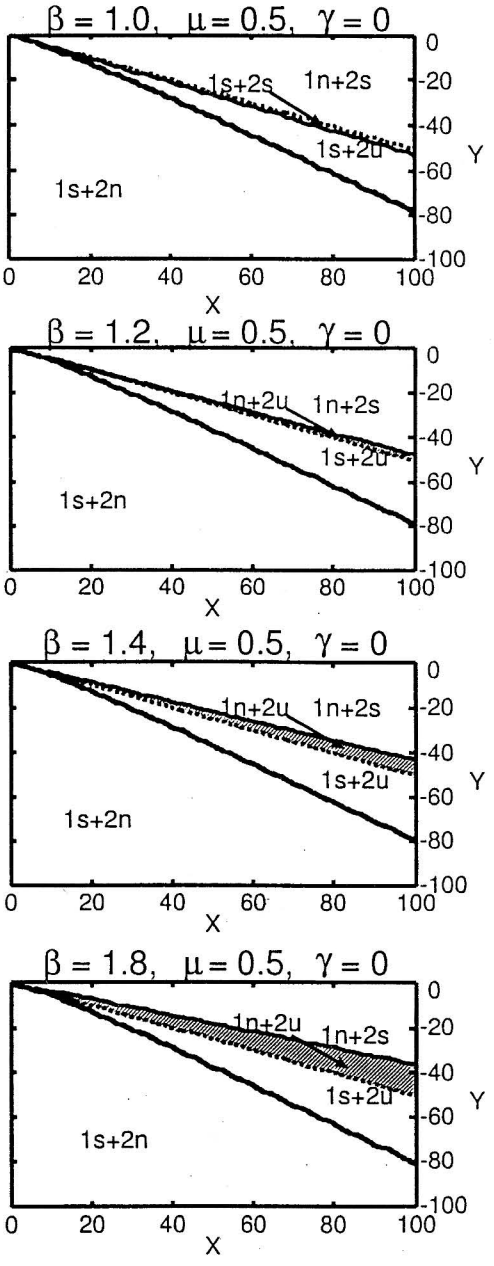

Fig. 7: Classification diagrams for the stability of (possibly stable) equilibrium states in the X-Y parameter space. Two primary regimes are clearly evident, one is the regime of intense NADW formation which has stable solutions when $-Y$ is relatively small, while the other is the stagnant NADW regime which has stable solutions when $-Y$ is relatively large. The numbers and letters employed to describe each of the distinct regions of "stability space" are employed to denote the stability of these two (possibly stable) equilibria in the corresponding region. The number 1 denotes the stagnant NADW state, whereas the number 2 denotes the intense NADW state. The letters, n, u and s indicate whether the solution is non-physical, unstable or stable. From top to bottom the individual "stability space" diagrams are for the sequence of β values 1.0, 1.2, 1.4, and 1.6

In Figure 7 the previously described results of the stability analysis are employed to classify the two possible equilibrium solutions in the X, Y plane for $\mu = 0.5$ and for 4 values of β. It is clearly evident in this Figure that the local stability of the possible equilibrium solutions is split into regimes by the condition $Y + \mu X = 0$. In this Figure, the nomenclature used to denote the stability of the two possible equilibria is as follows: the number 1 refers to the stagnant steady state, whereas the number 2 refers to the state of strong NADW, and each of these states is classified as being either s (steady), u (unsteady) or n (not physical).

Inspection of Figure 7 demonstrates that for $\beta = 1.2$ a Hopf bifurcation exists for a value of Y slightly smaller than $-\mu X$, so that the regime of intense NADW formation becomes unstable. Further inspection of Figure 7 will show that as β increases this Hopf bifurcation persists, while the slice of the X-Y plane in which the stagnant solution does not exist and the strong NADW solution is unstable expands. Because no stable equilibrium solution exists in this shaded region of the plane,the direct integration of the governing nonlinear ordinary differential equations will deliver either a limit cycle or deterministic chaos.

Figure 8 presents results for two such sample integrations of the dynamical system, each of which is initialized with values of (x, y, z) close to those corresponding to the equilibrium solution. The upper part of the Figure shows the result for $\beta = 1.4$, the lower for $\beta = 1.8$. In each case the values of X, Y and μ are fixed to 100, −45 and 0.5 respectively. An inspection of these sample results demonstrates that subsequent to an initial period of slow evolution, the solution assumes the form of a limit cycle in which NADW formation remains weak for the largest fraction of the cycle, a period followed by an intense burst of activity (the "flush"), followed in turn by a return to quasi quiescence (the "collapse"). This behavior is essentially identical to that exhibited by the previously discussed hydrodynamic model of the D-O oscillation in the ocean-only configurations analyzed in Sakai and Peltier (1995, 1996). Both models therefore embody the concept of the "salt oscillator" as first enunciated in Broecker et al. (1990). Furthermore, because this oscillation involves the same "flush-collapse" process previously observed in full 3-D models of ocean general circulation, it would appear to provide a fully robust explanation of the D-O oscillation which is such a prominent part of climate variability during OIS 3 in the GRIP and GISP2 ice cores from Summit, Greenland.

The essence of this oscillation is such that it involves the interaction between physical processes act-

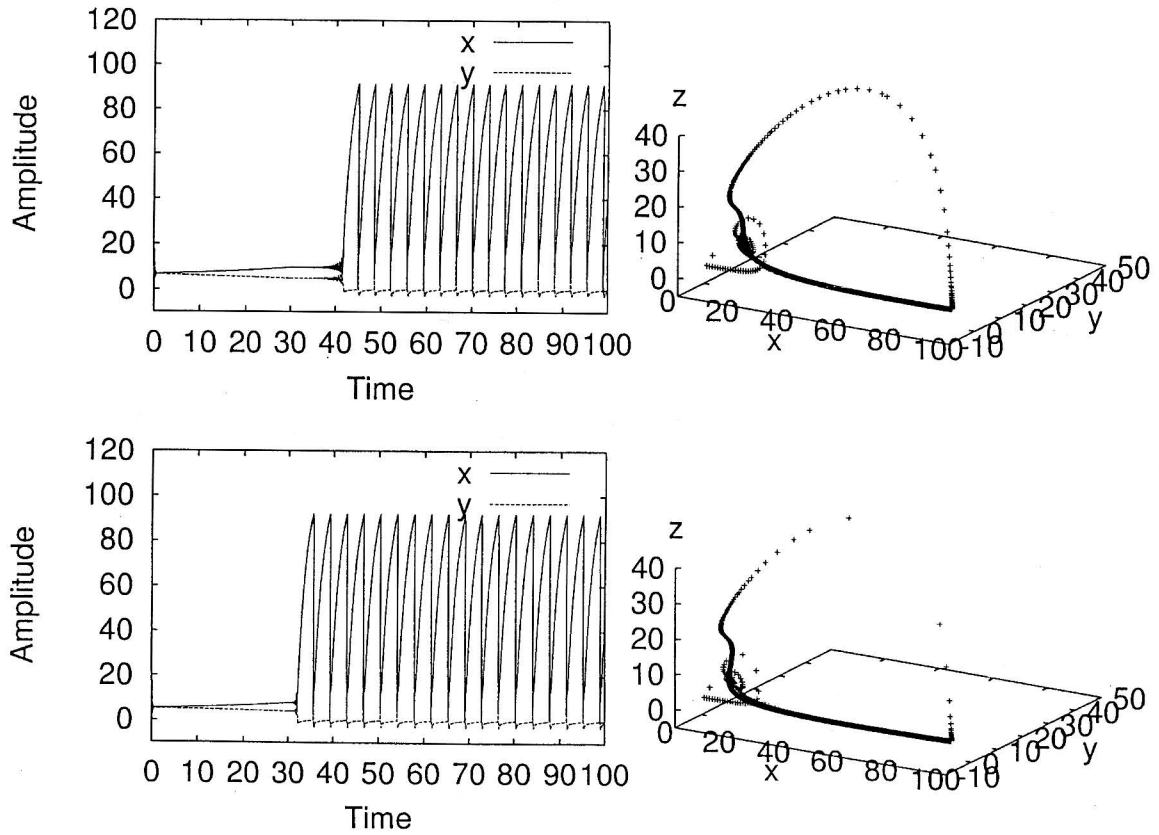

Fig. 8: Example time series from the regime in which both the stagnant NADW solution and the intense NADW solution are unstable for the two values of $\beta = 1.4$ (top) and $\beta = 1.8$ (bottom). These integrations illustrate the form of Dansgaard-Oeschger oscillation delivered by the new box model of THC

ing on two widely separated time scales, namely the "fast" process of convective instability and the "slow" process of diffusion. In the phase of oscillation in which convective destabilization of the water column occurs and neutralizes density stratification though NADW production, the potential density inversion is entirely eliminated. This defines the "flush" phase. The next flush cannot occur until the slow process of diffusion is able to reestablish the conditions acquired for convective instability in the high-latitude region. This long time scale defines the "collapse" phase of the oscillation. During this phase the salinity at the surface of the high-latitude Atlantic continues to increase by diffusion down the salinity gradient which becomes increasingly strong between low mid-latitudes, where salinity continuously increases due to the excess of evaporation over precipitation which characterizes this region. So long as high-latitude freshening is not too strong, this down gradient diffusion will eventually restore the high-latitude density structure to the convectively instable state required to support the next "flush".

Conclusions

Although the analyses reviewed above do indeed appear to provide a clear explanation of the D-O oscillation itself, they clearly do not suffice to explain why it is structured into the successive Bond cycles discussed in the introduction. In Sakai and Peltier (1999) a sequence of further analyses has been performed which we believe to provide a highly satisfactory explanation of even this level of detail in the ice-core derived proxy climate observations. It seems clear to us that, although the Dansgaard-Oeschger oscillation itself would be expected to be sustained at approximately constant amplitude if anomalous freshwater forcing applied to the surface of the North Atlantic during the glacial stage were constant, this condition could not have obtained during OIS 3. This is clear on the basis of the observed Heinrich events, during which significant increases in freshwater forcing would have occurred. These Heinrich events are in fact instabilities of the cryosphere induced by the underlying D-O oscillation of the glacial

THC. The results presented in Sakai and Peltier (1999) demonstrate that a good facsimile of the Bond cycle can be created by simply modulating freshwater forcing on the time scale of these Heinrich events.

Acknowledgments

The research reported herein has been supported through the Canadian program in Climate System History and Dynamics which receives financial support from both the Natural Sciences and Engineering Research Council of Canada and the Atmospheric Environment Service of Canada and through NSERC grant A9627.

References

Bard, E. B., B. Hamelin, R. G. Fairbanks, and A. Zindler, Calibration of the ^{14}C time scale over the past 30,000 years using mass spectrometric U-Th ages from Barbados corals, *Nature*, 345, 405–409, 1990.

Baumgartner, A., and E. Reichel, *The World Water Balance*, 179 pp., Elsevier, New York, 1975.

Bond, G., W. Broecker, S. Johnsen, J. McManus, L. Labeyrie, J. Jouzel, and G. Bonani, Correlations between climate records from North Atlantic sediments and Greenland ice, *Nature*, 365, 143–147, 1993.

Bond, G., and R. Lotti, Iceberg discharges into the North Atlantic on millennial time scales during the last glaciation, *Science*, 267, 1005–1010, 1995.

Broecker, W. S., G. Bond, and M. Klas, A salt oscillator in the glacial Atlantic? 1. The concept, *Paleoceanogr.*, 5, 465–477, 1990.

Broecker, W. S., and G. Denton, The role of ocean-atmosphere reorganizations in glacial cycles, *Geochim. Cosmochim. Acta*, 53, 2465–2501, 1989.

Chappell, J., A. Omura, T. Esat, M. McCullock, J. Pandolfi, Y. Ota, and B. Pillans, Reconciliation of late Quaternary sea levels derived from coral terraces at Huon Peninsula with deep sea oxygen isotope records, *Earth Planet. Sci. Lett.*, 141, 227–236, 1996.

Deblonde, G., and W. R. Peltier, Simulations of continental ice sheet growth over the last glacial interglacial cycle: Experiments with a one level seasonal energy balance model including realistic geography, *J. Geophys. Res.*, 96, 9189–9215, 1991.

Deblonde, G., and W. R. Peltier, Late Pleistocene ice age scenarios based upon observational evidence, *J. Climate*, 6, 709–727, 1993.

Duplessy, J. - C., L. Labeyrie, A. Juillet-Leclerc, F. Maitre, J. Duprat, and M. Sarnthein, Surface salinity reconstruction of the North Atlantic Ocean during the last glacial maximum, *Oceanol. Acta*, 14, 311–324, 1991.

Fairbanks, R. G., A 17,000-year glacio-eustatic sea level record: Influence of glacial melting rates on the Younger-Dryas event and deep-ocean circulation, *Nature*, 342, 637–642, 1989.

Heinrich, H., Origin and consequences of cyclic ice rafting in the Northeast Atlantic Ocean during the past 130,000 years, *Quat. Res.*, 29, 142–152, 1988.

Johnsen, S. J., and Co-authors, Irregular glacial interstadials recorded in a new Greenland ice core, *Nature*, 359, 311–313, 1992.

Killworth, P. D., The mixing and spreading phase of MEDOC.1, *Prog. Oceanogr.*, 7, 59–90, 1976.

Peltier, W. R., and S. Marshall, Coupled energy balance/ice-sheet model simulations of the glacial cycle: A possible connection between terminations and terrigenous dust, *J. Geophys. Res.*, 100, 14269–14289, 1995.

Sakai, K., and W. R. Peltier, Oscillatory modes of behavior in a simple model of the Atlantic thermohaline circulation, in *Ice in the Climate System*, edited by W. R. Peltier, pp. 459–480, NATO ASI Ser. I-12, Springer-Verlag, Berlin, 1993.

Sakai, K., and W. R. Peltier, A simple model of the Atlantic thermohaline circulation: Internal and forced variability with paleoclimatological implications, *J. Geophys. Res.*, 100, 13455–13479, 1995.

Sakai, K., and W. R. Peltier, A multi-basin reduced model of the global thermohaline circulation: Paleoceanographic analyses of the origins of ice-age climate variability, *J. Geophys. Res.*, 101, 22535–22562, 1996.

Sakai, K., and W. R. Peltier, Dansgaard-Oeschger oscillations in a coupled atmosphere-ocean climate model, *J. Clim.*, 10, 949–970, 1997.

Sakai, K., and W. R. Peltier, Deglaciation induced climate variability: An explicit model of the glacial-interglacial transition that simulates both the Bølling/Allerød and Younger-Dryas events, *J. Meteorological Society of Japan*, 76, 1029–1044, 1998.

Sakai, K., and W. R. Peltier, A dynamical systems model of Dansgaard-Oeschger oscillation and the origin of the Bond cycle, J. Clim., 12, 2238–2255, 1999.

Shackleton, N. J., Oxygen isotopes, ice volume and sea level, *Quat. Sci. Rev.*, 6, 183–190, 1987.

Schutz, C., and W. L. Gates, Global climatic data for surface, 800 mb, 400 mb, January, July, *Advanced Research Projects Agency Report*, 1971.

Solheim, L. P., and W. R. Peltier, Heat transfer and the onset of chaos in an axisymmetric anelastic model of whole mantle convection, *Geophys. Astrophys. Fluid Dyn.*, 53, 205–255, 1990.

Stommel, H. M., Thermohaline convection with two stable regimes of flow, *Tellus*, XIII (2), 224–230, 1961.

Tarasov, L., and W. R. Peltier, Terminating the 100 kyr ice age cycle, *J. Geophys. Res.*, 102, 21665–21693, 1997.

Tarasov, L., and W. R. Peltier, The influence of thermomechanical ice-sheet coupling in a theory of the 100 kyr ice-age cycle, *J. Geophys. Res.*, 104, D8, 9517–9545, 1999.

Teller, J. T., Proglacial lakes and the southern margin of the Laurentide ice sheet, in *North America and Adjacent Oceans During the Last Deglaciation, Decade of North American Geology*, Vol. K-3, edited by W. E. Ruddiman, and H. E. Wright, pp. 39–69, Geological Society of America, Boulder, Colorado, 1987.

Uspensky, J. V., *Theory of Equations*, McGraw-Hill Book Co. Inc., New York, 1948.

Weaver, A. J., J. Marotzke, P. F. Cummins, and E. S. Sarachik, Stability and variability of the thermohaline circulation, *J. Phys. Oceanogr.*, 23, 39–60, 1993.

Winton, M., and E. S. Sarachik, Thermohaline oscillations induced by strong steady salinity forcing of an ocean general circulation model, *J. Phys. Oceanogr.*, 23, 1389–1410, 1993.